Low-lying level structure of the neutron-unbound $N = 7$ isotones

D. Votaw [1,2,*] P. A. DeYoung,[3] T. Baumann,[1] A. Blake,[4] J. Boone,[5] J. Brown,[6] D. Chrisman,[1,2] J. E. Finck,[7] N. Frank,[8]
J. Gombas,[3] P. Guèye,[4,†] J. Hinnefeld,[9] H. Karrick,[8,‡] A. N. Kuchera,[10] H. Liu,[1,2] B. Luther,[11] F. Ndayisabye,[1,2] M. Neal,[4]
J. Owens-Fryar,[12] J. Pereira,[1] C. Persch,[3] T. Phan,[10] T. Redpath,[1,2] W. F. Rogers,[13] S. Stephenson,[14] K. Stiefel,[1,15] C. Sword,[3]
A. Wantz,[5] and M. Thoennessen[1,2,§]

[1]*National Superconducting Cyclotron Laboratory, Michigan State University, East Lansing, Michigan 48824, USA*
[2]*Department of Physics and Astronomy, Michigan State University, East Lansing, Michigan 48824, USA*
[3]*Department of Physics, Hope College, Holland, Michigan 49422-9000, USA*
[4]*Department of Physics, Hampton University, Hampton, Virginia 23668, USA*
[5]*Division of Natural Sciences, Indiana Wesleyan University, Marion, Indiana 46953, USA*
[6]*Department of Physics, Wabash College, Crawfordsville, Indiana 47933, USA*
[7]*Department of Physics, Central Michigan University, Mount Pleasant, Michigan 48859, USA*
[8]*Department of Physics and Astronomy, Augustana College, Rock Island, Illinois 61201, USA*
[9]*Department of Physics and Astronomy, Indiana University South Bend, South Bend, Indiana 46634-7111, USA*
[10]*Department of Physics, Davidson College, Davidson, North Carolina 28035, USA*
[11]*Department of Physics, St. John's College, Annapolis, Maryland 21401, USA*
[12]*Department of Physics, Applied Physics, and Astronomy, Rensselaer Polytechnic Institute, Troy, New York 12180, USA*
[13]*Physics Department, Indiana Wesleyan University, Marion, Indiana 46953, USA*
[14]*Department of Physics, Gettysburg College, Gettysburg, Pennsylvania 17325, USA*
[15]*Department of Chemistry, Michigan State University, East Lansing, Michigan 48824, USA*

This article reports on results of an experimental search for ground state shell inversion in the neutron-unbound $N = 7$ isotones ^{9}He and ^{10}Li. Two different radioactive ion beams (^{11}Be, $E_{\rm lab} = 44$ MeV/u and ^{12}B, $E_{\rm lab} = 45$ MeV/u) impinging on a beryllium target were used to directly and selectively populate unbound states of a given ℓ in the nuclides of interest. Be(^{11}Be, ^{8}He $+n$) and Be(^{12}B, ^{8}He $+n$) reactions populated unbound states in ^{9}He. Fragments and neutrons were detected in coincidence to reconstruct the decay energy of ^{9}He using invariant mass spectroscopy. Similarly, Be(^{11}Be, ^{9}Li $+n$) and Be(^{12}B, ^{9}Li $+n$) reactions were used to populate unbound states in ^{10}Li, and the time-of-flight method was used to determine the relative velocity of the ^{9}Li fragments and neutrons in coincidence. Various states in both ^{9}He and ^{10}Li were observed and characterized. The data indicate possible ground state shell inversion in both cases.

I. INTRODUCTION

Experimental studies of the properties of atomic nuclei far from stability have become an active area of research in the past decades due to the availability of radioactive ion beams at various facilities around the world [1]. Of particular interest in this paper is the evolution of nuclear shell structure towards the extremes of N/Z, even beyond the neutron drip line. Experimentally determining the structure of highly exotic nuclides places strong constraints on theoretical models of

nuclear structure and forces. The unbound $N = 7$ isotones are particularly interesting given their proximity to the "light island of inversion" around ^{11}Li and ^{11}Be [2–9].

In a naïve approach to modeling the ground state structure of an $N = 7$ nuclide, one might assume that the first six neutrons fill the $\nu(1s_{1/2})$ and $\nu(1p_{3/2})$ orbitals, leaving the single valence neutron to occupy a $\nu(1p_{1/2})$ orbital. However in the case of ^{11}Be, it is known that the ground state contains a strong $\nu(2s_{1/2})$ component, evident by its halo structure [10–13]. Some calculations have suggested that ^{9}He and ^{10}Li should have a similar neutron structure in their ground states [8,14,15], although there is still some theoretical disagreement [16]. Previous experiments have not yet provided a consistent picture of the ground state structure of either ^{9}He [17–28] or ^{10}Li [20,29–47].

Early experimental studies of ^{9}He [17–20] assigned a ground state J^π of $\frac{1}{2}^-$ for a state which was observed at about 1 MeV above the neutron threshold. However later works [21,23,24,27] suggest that this $\frac{1}{2}^-$ state may actually

be an excited state, and that an even lower $\frac{1}{2}^+$ state is the ground state. In the 2001 knockout experiment of Chen *et al.* [21], it was first suggested that a low-lying *s*-wave virtual state had been observed with scattering length $a_s < -10$ fm. However, this work was not able to simultaneously constrain the $\frac{1}{2}^-$ and confirm ground state inversion. Subsequent direct measurements using transfer reactions [23,24,27] support the conclusion of Chen *et al.*, but indirect measurements using elastic scattering [22,28] disagree with it. Another knockout experiment, at a much higher beam energy, was performed in 2010 by Johansson *et al.* [25], where an observation of an *s*-wave neutron interaction with a scattering length of $-3.17(66)$ fm was suggested. While the knockout experiments of both Chen and Johansson provided evidence for an *s*-wave decay, they disagree on the value of the scattering length and the physical interpretation. It was suggested by Johansson *et al.* that their observation was a threshold effect rather than a true state, due to the small magnitude of the scattering length and the reaction mechanism used. On the other hand, Chen *et al.* suggested an observation of a low-lying, narrow virtual state. In 2011, Al Falou *et al.* reported another knockout measurement performed at GANIL which seemed to agree with Johansson [26].

In the case of ^{10}Li, some experiments have provided evidence for an *s*-wave neutron configuration in the ground state [20,29–31,33–35,39,40,42,43,48], while others have not [32,36–38,41,44–47]. However, there is fairly good agreement among previous experiments that there is a *p*-wave neutron state at about ≈ 0.5 MeV [33–37,39,42–47,49]. Many of the previous experimental works on both ^{9}He and ^{10}Li suffer from poor statistics and signal-to-background ratios, making the results and conclusions somewhat uncertain.

In this work, two different beams were used to selectively populate states in ^{9}He and ^{10}Li, based on the neutron structure of the isotope. This technique has been well characterized in previous works [21,34]. ^{11}Be is a well-known halo nucleus, where the valence neutron primarily occupies an *s* orbital. Thus direct removal of one or two protons from ^{11}Be beam would be expected to populate ^{10}Li or ^{9}He with the valence neutron primarily occupying an *s* orbital. ^{12}B is a nonhalo nucleus, and the valence neutron primarily occupies a *p* orbital. Direct removal of two or three protons would be expected to populate ^{10}Li or ^{9}He with the valence neutron primarily occupying a *p* orbital. Selectively populating these states with the two separate beams using the same experimental setup should allow for a determination of the ordering of the states in the level scheme.

II. EXPERIMENT

This experiment was performed at the National Superconducting Cyclotron Laboratory. Two different secondary beams of ^{11}Be and ^{12}B were developed. The Coupled Cyclotron Facility [50] provided a 120 MeV/u ^{18}O beam which was impinged on a beryllium production target, of thickness 2938 mg/cm^2 for the ^{11}Be beam and 3525 mg/cm^2 for the ^{12}B beam. The secondary beams of interest were produced using in-flight projectile fragmentation, and unwanted contaminants

were filtered out by the A1900 Fragment Separator [51]. The two secondary beams were transported to the experimental area in the N2 vault (Fig. 1).

In the experimental area, the ^{11}Be and ^{12}B secondary beams were directed onto a beryllium reaction target with a thickness of 188 mg/cm^2. Within the reaction target, the reactions Be(^{11}Be, ^{8}He $+n$), Be(^{12}B, ^{8}He $+n$), and Be(^{11}Be, ^{9}Li $+n$), Be(^{12}B, ^{9}Li $+n$) were used to populate unbound ^{9}He and ^{10}Li, respectively. These unbound states then immediately decayed ($t_{1/2} \approx 10^{-21}$ s) by one-neutron emission to the bound nuclides ^{8}He or ^{9}Li. After the decay, the fragments entered a large-gap dipole Sweeper magnet [52], where they were swept 43.3° into a vacuum chamber containing multiple charged particle detectors, and the undeflected neutrons traveled along a ≈ 6 meter flight path and into the Modular Neutron Array (MoNA) [53] and Large multi-Institutional Scintillator Array (LISA).

MoNA-LISA is an array of (10 cm $\times$ 10 cm $\times$ 2 m) BC-408 scintillator bars, with a photomultiplier tube (PMT) at each end. 272 of the 288 MoNA-LISA bars were used for this experiment, stacked in 17 layers of 16 bars. Timing and light output signals are recorded from each of the 544 PMTs. The array is segmented in height and depth, and the position of an event in the lengthwise direction along the bar is determined from the time difference between signals in the two PMTs on the bar in which the interaction occurred. A three-dimensional position vector relative to the target is determined for every valid interaction in MoNA-LISA. Using the difference between the timing signal in the scintillator bar (the average of the two PMTs) and the timing signal from the target scintillator, the neutron time of flight from target to interaction point is measured. Using the time of flight and position of the interaction in MoNA-LISA, the full four-momentum vector of the neutron is determined. Prompt neutron interactions in MoNA-LISA were discriminated from background γ rays and cosmic muons by requiring a coincidence with a fragment and using a time-of-flight gate in software.

The charged particle detection chamber contains two cathode readout drift chambers (CRDCs) [54] separated by 1.55 m, an ionization chamber, and a thin timing scintillator. The Sweeper magnet current was set so that particles with the average magnetic rigidity of the ^{8}He fragments move along the design trajectory through the dipole and into the detection chamber. The CRDCs are position sensitive in both transverse directions. Using the two CRDCs, positions and angles of the charged fragments in the dispersive and nondispersive planes of the Sweeper magnet were measured. The ionization chamber measured the energy loss of the fragment as it traversed its active volume. The final timing scintillator was used to measure the time of flight of the fragment relative to the target scintillator, as well as acting as the trigger for the entire system of the Sweeper and MoNA-LISA detectors.

Element identification was done with ΔE-ToF from the ionization chamber and the timing scintillators. Once element identification was completed, a software gate was used to select only events where the desired element is transmitted to the charged particle detectors (Fig. 2). Individual isotopes were identified using the positions and angles of the charged particles in the dispersive direction at the CRDCs, and the
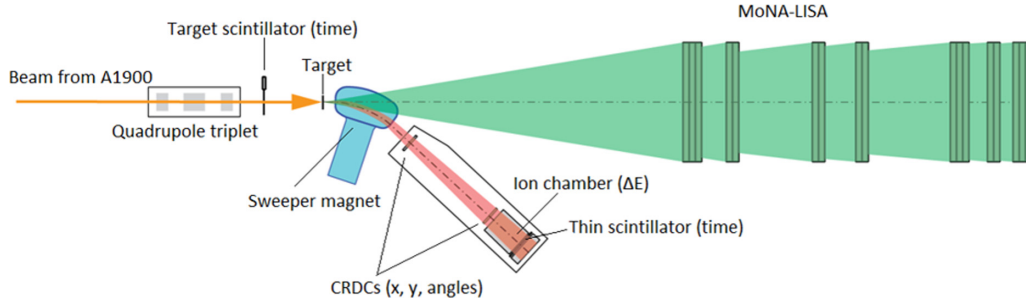
FIG. 1. The schematic layout of the experimental setup in the N2 vault. The green shaded areas represent the neutron acceptance cones of each layer in MoNA-LISA.

time of flight from the target to the final timing detector. The ^{8}He fragments were isolated by correcting the time of flight for the dispersive positions and angles to obtain separation by A/Z ratio. Because the fractional differences in A/Z along the helium isotopic chain are large, and the heavy odd-N helium isotopes are unbound, the ^{8}He only needed to be separated from ^{6}He. The same procedure was applied to the slightly more difficult case of the lithium isotopes (Fig. 3), where ^{9}Li, ^{8}Li, and a small amount of ^{7}Li are within the Sweeper acceptance. After isotope identification was completed, a software gate was created to isolate events where the desired fragment was detected. Third-order ion-optical calculations using COSY INFINITY [55] were used to relate the measured transverse positions and angles of the ^{8}He fragments in the CRDCs to the transverse angles and energy of the fragments before entering the Sweeper magnet [56]. Energy loss calculations using LISE++ [57] were used to add back the energy lost by the fragments over the target thickness assuming the knockout reaction and neutron decay occur in the center of the reaction target. Thus, the full four-momentum of the ^{8}He fragment immediately after the ^{9}He decay was determined. From the four-momenta of the neutron and ^{8}He fragment, the decay energy [Eq. (1)] of ^{9}He was reconstructed event by event for each secondary beam particle:

$$E_d = \sqrt{m_f^2 + m_n^2 + 2(E_f E_n - \vec{p}_f \cdot \vec{p}_n)} - m_f - m_n. \quad (1)$$
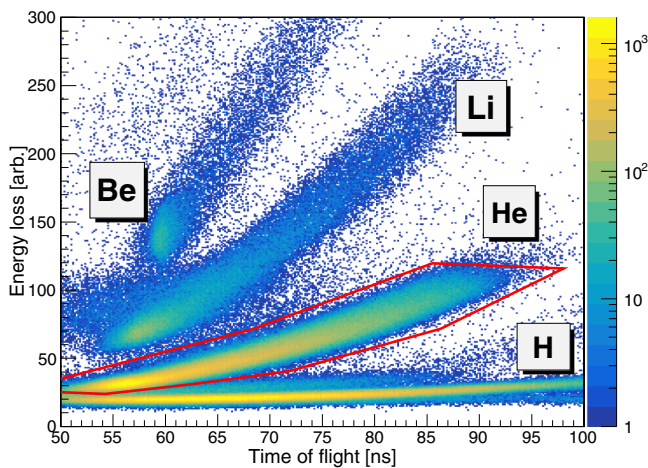
In the case of ^{10}Li, the average rigidity of the ^{9}Li fragments is far from the central rigidity of the Sweeper magnet [$\Delta(B\rho)/B\rho \approx 25\%$], so the COSY reconstruction is not reliable. Instead of calculating the decay energy, the relative velocity [Eq. (2)] can be calculated without the fragment angles at the target location, simply using the fragment speed, which is measured using the time of flight (ToF) between the target and thin scintillators. The path length of the ^{9}Li trajectory through the Sweeper magnet is not known on an event-by-event basis, so it is fixed to a constant value such that the peak of the relative velocity distribution is fixed to zero, within uncertainties:

$$v_{\rm rel} \equiv |\vec{v}_n| - |\vec{v}_f| \quad (2)$$

The experimental efficiencies as a function of decay energy and relative velocity for the ^{11}Be beam are shown in Figs. 4 and 5, respectively. The efficiency curves for the ^{12}B beam are very similar.

III. DATA ANALYSIS

Extraction of resonance parameters from the experimental data was done by comparison with Monte Carlo simulations. An in-house simulation package, coupled with GEANT4 and the MENATE_R neutron physics package [58], was used to simulate the phase space evolution of the beam, the knockout reactions in the target, the subsequent one-neutron decays, the propagation of the charged fragments through the Sweeper
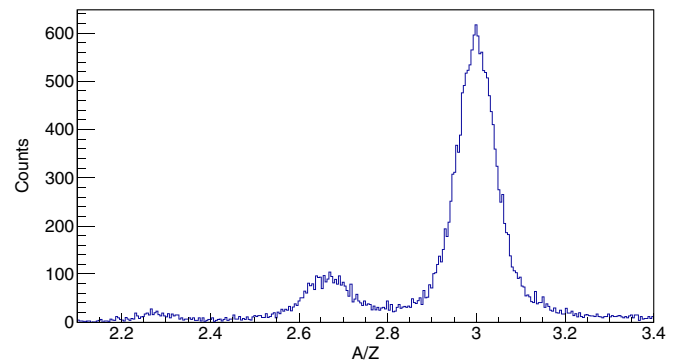

FIG. 2. Helium identification gate for the ^{11}Be secondary beam.

FIG. 3. Lithium isotope identification for the ^{11}Be secondary beam. The two main peaks are ^{8}Li and ^{9}Li.
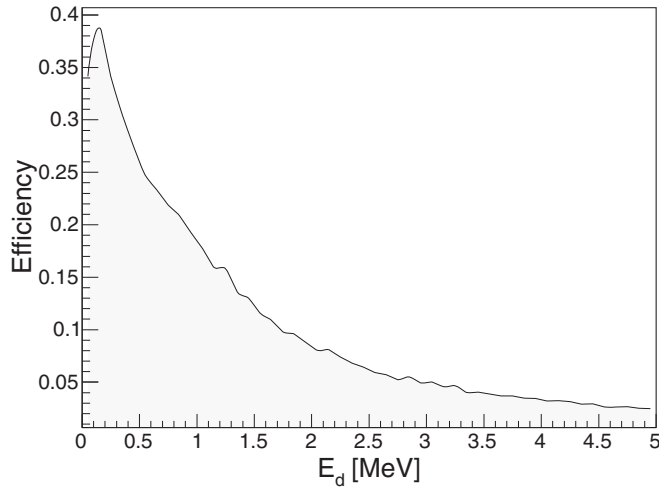
FIG. 4. Experimental response as a function of decay energy for the ^{11}Be beam.

FIG. 6. Decay energy spectrum from Be(^{12}B, ^{8}He $+n$).

magnet, and the propagation of the neutrons into MoNA-LISA (including acceptances and detector responses). The simulated pseudodata were subjected to the same analysis as the experimental data, and a maximum likelihood fit was performed to extract best estimates of the parameters for the neutron decay line shapes and their statistical uncertainties. Systematic uncertainties were estimated by varying input parameters of the analysis over a physically reasonable range and determining the magnitude of their effects on the location of the likelihood.

The line shape for the simulated *s*-wave decay was taken from Refs. [48,59], and the line shapes for decays with $\ell > 0$ were assumed to take the form of a single-level asymmetric Breit-Wigner distribution [60]:

$$\sigma_\ell(E) \propto \frac{\Gamma_\ell}{(E_0 - E + \Delta_\ell)^2 + \frac{1}{4}\Gamma_\ell^2} \qquad (3)$$

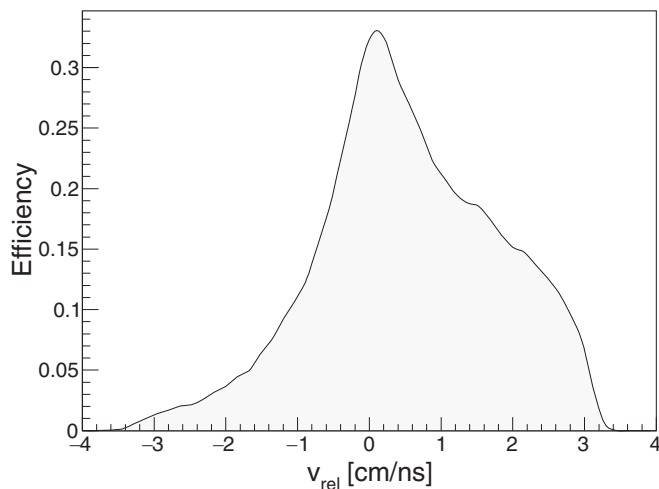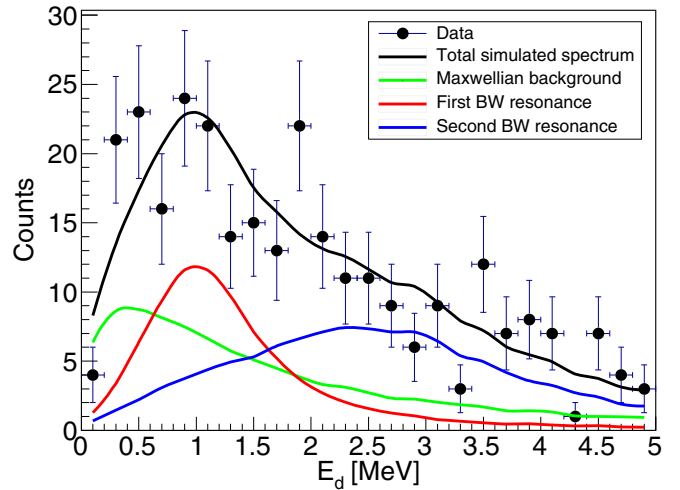FIG. 5. Experimental response as a function of relative velocity for the ^{11}Be beam.

The *s*-wave line shape has three parameters: a scattering length, an effective range, and a binding energy which is dependent on the initial state (in this case, the ground state of ^{11}Be). The binding energy parameter is fixed to the one-neutron separation energy of ^{11}Be [48], so the scattering length and effective range are the only free parameters for this line shape. Because the shape of the distribution is insensitive to the effective range parameter [59], it was fixed at 3 fm for this analysis, leaving only the scattering length as a fitting parameter. The line shapes for $\ell > 0$ are each parametrized by a resonance energy and decay width.

In addition to the decays of low-lying unbound states, there may be other processes which produce a neutron in coincidence with the fragment of interest, as discussed in Ref. [21]. These contributions make up the experimental background. In order to simulate the background, a Maxwellian line shape of the form $\sqrt{E}e^{-E/\Theta}$, with a single free parameter Θ, was used. This is a standard background model, used in many similar analyses [61–69].

A. ^{9}He results

The decay energy spectrum from the Be(^{12}B, ^{8}He $+n$) reaction (Fig. 6) was fit with a combination of two Breit-Wigner (BW) resonances and a Maxwellian background (MB). It was found that a Maxwellian background plus two resonances was required to fit the observed spectrum, as a pure Maxwellian or a Maxwellian plus one resonance could not adequately fit the spectrum over the whole range of decay energies. The maximum log-likelihoods for pure MB and MB + 1BW deviate from the MB + 2BW maximum by 2.5σ and 1.5σ, respectively. The first resonance is a *p* wave with a resonance energy of $1.1^{+0.7}_{-0.4}$ MeV ($\Gamma > 1.3$ MeV). The second resonance is a *p* wave with energy $3.1^{+1.0}_{-0.8}$ MeV ($\Gamma > 1.7$ MeV). Although a *p*-wave lines hape was used for the higher resonance in the final fit, a *d* wave could have been used instead with little change in the value of the likelihood or the other fit parameters. Because no states of $J > \frac{5}{2}$ are expected in the relevant range of excitation energies, the second resonance
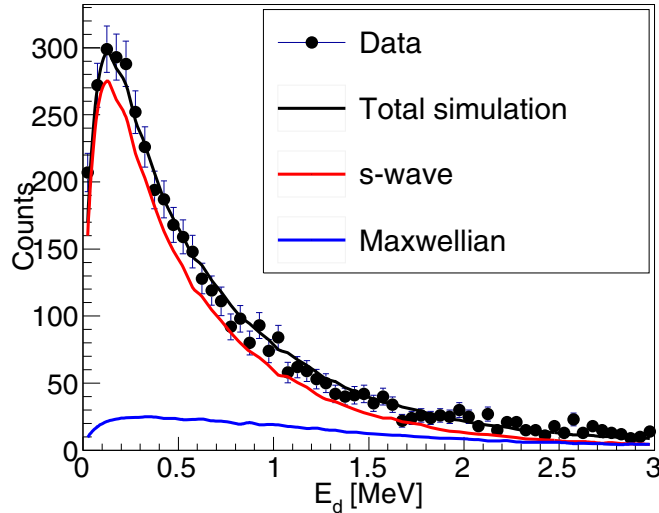
FIG. 7. Decay energy spectrum from Be(^{11}Be, ^{8}He $+n$), fit with an $a_s = -2$ fm s wave and a small Maxwellian contribution.

is tentatively assigned an ℓ of 1 or 2. The decay energy resolutions (FWHM) for this measurement at 1 and 3 MeV are 500 and 800 keV, respectively. At the likelihood maximum, the Maxwellian $\Theta = 3.5$ MeV.

For the Be(^{11}Be, ^{8}He $+n$) reaction, the decay energy and relative velocity spectra were fit with a combination of an s-wave line shape and a Maxwellian background. The fitting resulted in two distinct likelihood maxima differing by less than 1σ in significance. One of the maxima is a combination of a wide s wave and a weak Maxwellian background (Fig. 7), and the other consists of a narrow s wave and a stronger background (Fig. 8). The Maxwellian Θ parameters also differ at the two maxima ($\Theta = 2.5$ MeV with the wide s wave and $\Theta = 1.5$ MeV with the narrow s wave).

The values of the scattering lengths at the two likelihood maxima are -2.1 ± 0.6(stat.) $\pm$ 0.2(syst.) fm and -6.8 ± 1.2(stat.) $\pm$ 0.7(syst.) fm.

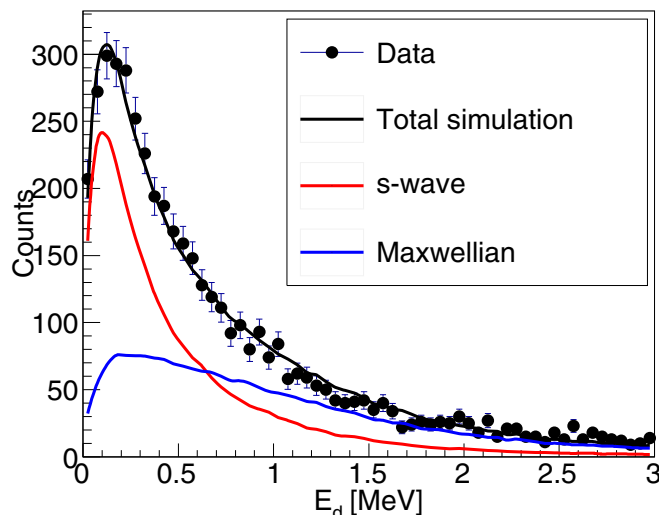

FIG. 8. Decay energy spectrum from Be(^{11}Be, ^{8}He $+n$), fit with an $a_s = -7$ fm s wave and a larger Maxwellian contribution.
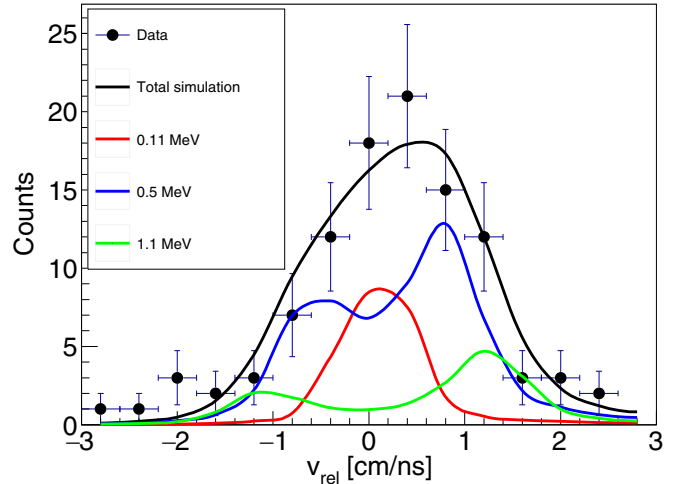

FIG. 9. Relative velocity spectrum from Be(^{12}B, ^{9}Li $+n$). The points are data from the current experiment, and the curves are simulations based on the results of Smith [44,49].

B. ^{10}Li results

For ^{10}Li, the ToF method was used to reconstruct the relative velocity of the ^{9}Li fragment and neutron. A discussion of what various line shapes look like in the relative velocity spectrum is given in Ref. [39]. The Be(^{12}B, ^{9}Li $+n$) data were used to verify the ToF method, because this exact reaction was studied previously using the invariant mass method by Smith [44,49], using the same experimental setup. Three previously known $\ell = 1$ resonances from Refs. [44,49] were simulated, and the spectrum was overlaid with the experimental data from this work, as shown in Fig. 9. The simulated resonances had energies of 0.11 MeV (0.2 MeV width, 13% population), 0.5 MeV (0.8 MeV width, 55% population), and 1.1 MeV (1 MeV width, 32% population).

The agreement between the two experiments using a very similar experimental setup demonstrates that the ToF method is able to reproduce previously known states in ^{10}Li, and suggests that it can be reliably applied to the Be(^{11}Be, ^{9}Li $+n$) data.

Similarly to the case of ^{9}He from the ^{11}Be beam, the experimental data can be fit with two distinct likelihood maxima: one with a wide s wave ($a_s = -1.4 \pm 1.0$ fm) and a weaker background (shown in Fig. 10), and one with a narrow s wave ($a_s = -7.0 \pm 2.4$ fm) and a stronger background (shown in Fig. 11). Both maxima have the same value of the Maxwellian parameter, $\Theta = 1$ MeV.

IV. DISCUSSION

The Be(^{12}B, ^{8}He $+n$) data suggest that there is a relatively low-lying p-wave resonance at about 1 MeV, and a higher-lying resonance at about 3 MeV. Due to the high energy and width of the higher-lying resonance, the p-wave and d-wave line shapes cannot be strongly distinguished. A p-wave line shape was assumed for the analysis, although a d-wave line shape would fit the data similarly well. From both theoretical and previous experimental level schemes, no resonances with dominant partial waves of $\ell > 2$ are expected to contribute
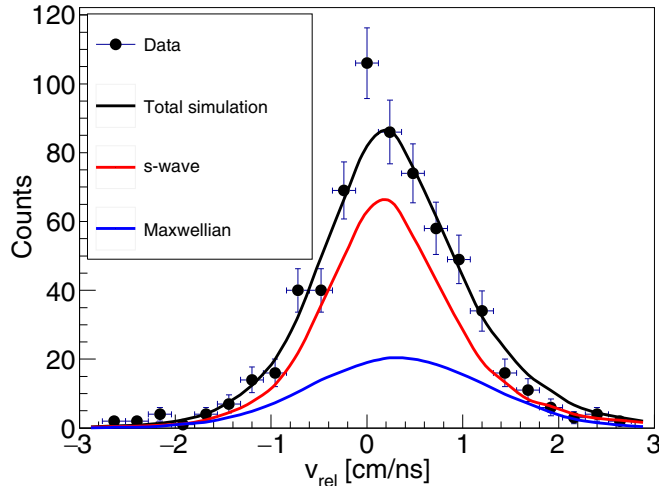
FIG. 10. Relative velocity spectrum from Be(^{11}Be, ^{9}Li $+n$), fit with an $a_s = -1$ fm *s* wave and a small Maxwellian contribution.

within the range of decay energies to which this experiment was sensitive. The use of a *p* or *d* line shape for the higher resonance does not affect the values of the other fitted parameters in a statistically significant way.

The presence of a *p*-wave resonance at about 1 MeV above the ^{8}He ground state is in close agreement with multiple previous experiments [17–20,22,23,25–27]. The single-particle width for this state was estimated by Bohlen *et al.* to be in the range of 1.5–2.0 MeV [20], which is slightly above the 1σ lower limit observed in this work. The spin and parity assignments of the higher-lying excited resonances vary greatly in the experimental literature, although many works agree that $J = \frac{3}{2}$ and/or $J = \frac{5}{2}$ excited levels exist in the ≈2–5 MeV range [17–20,22,24,27].

The Be(^{12}B, ^{9}Li $+n$) data are consistent with the three *p*-wave resonances observed by Smith [49], which demonstrates that the ToF method can reliably be applied to the ^{10}Li events observed in the current experiment.
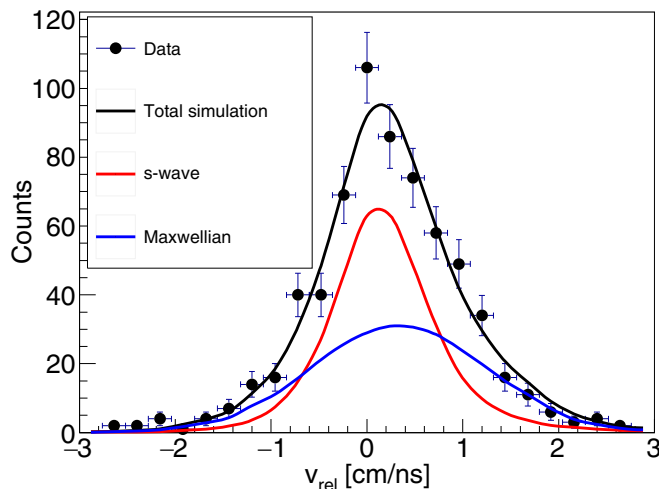

FIG. 11. Relative velocity spectrum from Be(^{11}Be, ^{9}Li $+n$), fit with an $a_s = -7$ fm *s* wave and a larger Maxwellian contribution.

The presence of an *s*-wave decay in ^{9}He is also in agreement with multiple experiments that were sensitive to it [21,23–27], although among those experiments there is disagreement about the value of the scattering length. The observation of an *s* state is also in disagreement with some previous experiments [17–19,28]. It has been suggested that the earliest of these experiments [17–19] may have been insensitive to a low-lying *s* state due to the reaction mechanisms used [21]. However, the more recent indirect measurement by Uberseder *et al.* [28] did not observe any low-lying *s* state.

In the current analysis, the Be(^{11}Be, ^{8}He $+n$) data can be fit with two different options of different scattering lengths. The large-$|a_s|$ result is qualitatively more consistent with the observation of Chen *et al.* [21] and Al Kalanee *et al.* [27], while the small-$|a_s|$ result is more consistent with Johansson *et al.* [25], Al Falou *et al.* [26], and Uberseder *et al.* [28]. The experimental method applied in the current work is very similar to that of Chen; however, the background models used were different. In the Chen *et al.* analysis of Be(^{11}Be, ^{8}He $+n$), the background contribution was modeled using event mixing, while in the current work a Maxwellian function was used. Because event mixing models uncorrelated coincidences between the fragment and neutron, the Maxwellian function is a more realistic background model. Using the Maxwellian function allows a larger parameter space to be searched in the likelihood maximization, which explains why the low-$|a_s|$ likelihood maximum was not found in the Chen analysis.

It has been argued in Refs. [1,70] that observed *s*-wave decays with $a_s \lesssim -5$ fm can be considered true *s* states in the nuclide of interest, while *s*-wave decays with $a_s \gtrsim -5$ fm cannot be distinguished from nonresonant final state interactions. So the $a_s = -7$ fm option can be considered a true *s* state in ^{9}He with the corresponding energy lying well below the 1 MeV *p* state, consistent with ground state shell inversion. However the $a_s = -2$ fm option should not be considered a low-lying *s* state, and an observation of ground state shell inversion cannot be claimed.

The Be(^{11}Be, ^{9}Li $+n$) data from this work can also be fit two different ways, the large-$|a_s|$ option being consistent with shell inversion, and the small-$|a_s|$ result being inconsistent with shell inversion, by the same argument as in the ^{9}He case. The large-$|a_s|$ option is qualitatively consistent with Kryger *et al.* [31], which was a very similar measurement to the Chen ^{9}He experiment. However the small-$|a_s|$ option is also consistent with previous works which did not observe shell inversion in ^{10}Li.

V. SUMMARY

In this work, neutron decays have been observed from various unbound states in ^{9}He and ^{10}Li. Assignments of resonance energies, widths, and spin and parity quantum numbers have been made where possible. *s*-wave decays from both nuclides have been observed, and their scattering lengths have been characterized. Two possibilities for the *s*-wave scattering lengths are given in each case. The values of the possible scattering lengths are ambiguous as to whether or not ^{9}He and ^{10}Li are inverted in the ground state. So the long-standing

debates about their ground state inversion remain unresolved. While a definitive answer has not yet been provided, this work has begun to elucidate the discrepancies between previous experimental analyses.

ACKNOWLEDGMENTS

[1] T. Baumann, A. Spyrou, and M. Thoennessen, Rep. Prog. Phys. **75**, 036301 (2012).

[2] M. V. Zhukov, B. V. Danilin, D. V. Fedorov, J. M. Bang, I. J. Thompson, and J. S. Vaagen, Phys. Rep. **231**, 151 (1993).

[3] S. Shimoura, T. Nakamura, M. Ishihara, N. Inabe, T. Kobayashi, T. Kubo, R. H. Siemssen, I. Tanihata, and Y. Watanabe, Phys. Lett. B **348**, 29 (1995).

[4] A. A. Korsheninnikov et al., Phys. Rev. C **53**, R537 (1996).

[5] S. Aoyama, Phys. Rev. Lett. **89**, 052501 (2002).

[6] I. Tanihata, M. Alcorta, D. Bandyopadhyay, R. Bieri, L. Buchmann, B. Davids et al., Phys. Rev. Lett. **100**, 192502 (2008).

[7] R. Kanungo, A. Sanetullaev, J. Tanaka, S. Ishimoto, G. Hagen, T. Myo et al., Phys. Rev. Lett. **114**, 192502 (2015).

[8] K. Fossez, J. Rotureau, and W. Nazarewicz, Phys. Rev. C **98**, 061302(R) (2018).

[9] D. Votaw, N = 7 shell evolution at and beyond the neutron dripline, Ph.D. thesis, Michigan State University, 2019, (unpublished), https://publications.nscl.msu.edu/thesis/%20Votaw_2019_6006.pdf

[10] P. G. Hansen, A. S. Jensen, and B. Jonson, Annu. Rev. Nucl. Part. Sci. **45**, 591 (1995).

[11] J. H. Kelley, S. M. Austin, R. A. Kryger, D. J. Morrissey, N. A. Orr, B. M. Sherrill, M. Thoennessen, J. S. Winfield, J. A. Winger, and B. M. Young, Phys. Rev. Lett. **74**, 30 (1995).

[12] S. Fortier et al., Phys. Lett. B **461**, 22 (1999).

[13] T. Aumann, A. Navin, D. P. Balamuth, D. Bazin, B. Blank, B. A. Brown, J. E. Bush, J. A. Caggiano, B. Davids, T. Glasmacher, V. Guimarães, P. G. Hansen, R. W. Ibbotson, D. Karnes, J. J. Kolata, V. Maddalena, B. Pritychenko, H. Scheit, B. M. Sherrill, and J. A. Tostevin, Phys. Rev. Lett. **84**, 35 (2000).

[14] P. G. Hansen and B. M. Sherrill, Nucl. Phys. A **693**, 133 (2001).

[15] C. R. Hoffman, B. P. Kay, and J. P. Schiffer, Phys. Rev. C **89**, 061305(R) (2014).

[16] M. Vorabbi, A. Calci, P. Navrátil, M. K. G. Kruse, S. Quaglioni, and G. Hupin, Phys. Rev. C **97**, 034314 (2018).

[17] K. K. Seth, M. Artuso, D. Barlow, S. Iversen, M. Kaletka, H. Nann, B. Parker, and R. Soundranayagam, Phys. Rev. Lett. **58**, 1930 (1987).

[18] H. G. Bohlen, B. Gebauer, D. Kolbert, W. von Oertzen, E. Stiliaris, M. Wilpert, and T. Wilpert, Z. Phys. A **330**, 227 (1988).

[19] W. von Oertzen et al., Nucl. Phys. A **588**, c129 (1995).

[20] H. G. Bohlen, A. Blazevič, B. Gebauer, W. V. Oertzen, S. Thummerer, R. Kalpakchieva, S. M. Grimes, and T. N. Massey, Prog. Part. Nucl. Phys. **42**, 17 (1999).

[21] L. Chen, B. Blank, B. A. Brown, M. Chartier, A. Galonsky, P. G. Hansen, and M. Thoennessen, Phys. Lett. B **505**, 21 (2001).

[22] G. V. Rogachev et al., Phys. Rev. C **67**, 041603(R) (2003).

[23] S. Fortier et al., in International Symposium on Exotic Nuclei, 17–22 July 2006, Khanty-Mansiysk, Russia, edited by Yu. E. Penionzhkevich and E. A. Cherepanov, AIP Conf. Proc. No. 912 (AIP, New York, 2007), p. 3.

[24] M. S. Golovkov, L. V. Grigorenko, A. S. Fomichev, A. V. Gorshkov, V. A. Gorshkov, S. A. Krupko et al., Phys. Rev. C **76**, 021605(R) (2007).

[25] H. T. Johansson et al., Nucl. Phys. A **842**, 15 (2010).

[26] H. A. Falou, A. Leprince, and N. A. Orr, J. Phys.: Conf. Ser. **312**, 092012 (2011).

[27] T. Al Kalanee, J. Gibelin, P. Roussel-Chomaz, N. Keeley, D. Beaumel, Y. Blumenfeld et al., Phys. Rev. C **88**, 034301 (2013).

[28] E. Uberseder et al., Phys. Lett. B **754**, 323 (2016).

[29] K. H. Wilcox, R. B. Weisenmiller, G. J. Wozniak, N. A. Jelley, D. Ashery, and J. Cerny, Phys. Lett. B **59**, 142 (1975).

[30] A. I. Amelin, M. G. Gornov, and Yu. B. Gurov, Yad. Fizika **52**, 1231 (1990) [Sov. J. Nucl. Phys. **52** (1990)].

[31] R. A. Kryger et al., Phys. Rev. C **47**, R2439 (1993).

[32] H. G. Bohlen et al., Z. Phys. A **344**, 381 (1993).

[33] B. M. Young et al., Phys. Rev. Lett. **71**, 4124 (1993).

[34] M. Zinser et al., Phys. Rev. Lett. **75**, 1719 (1995).

[35] M. Zinser et al., Nucl. Phys. A **619**, 151 (1997).

[36] T. Kobayashi, K. Yoshida, A. Ozawa, I. Tanihata, A. Korsheninnikov, E. Nikolski, and T. Nakamura, Nucl. Phys. A **616**, 223 (1997).

[37] H. G. Bohlen et al., Nucl. Phys. A **616**, 254 (1997).

[38] J. A. Caggiano, D. Bazin, W. Benenson, B. Davids, B. M. Sherrill, M. Steiner, J. Yurkon, A. F. Zeller, and B. Blank, Phys. Rev. C **60**, 064322 (1999).

[39] M. Thoennessen et al., Phys. Rev. C **59**, 111 (1999).

[40] M. Chartier et al., Phys. Lett. B **510**, 24 (2001).

[41] P. Santi et al., Phys. Rev. C **67**, 024606 (2003).

[42] H. B. Jeppesen et al., Phys. Lett. B **642**, 449 (2006).

[43] H. Simon et al., Nucl. Phys. A **791**, 267 (2007).

[44] J. K. Smith et al., Nucl. Phys. A **940**, 235 (2015).

[45] B. A. Chernyshev, Y. B. Gurov, L. Y. Korotkova, S. V. Lapushkin, R. V. Pritula, and V. G. Sandukovsky, Int. J. Mod. Phys. E **24**, 1550004 (2015).

[46] A. Sanetullaev et al., Phys. Lett. B **755**, 481 (2016).

[47] M. Cavallaro, M. DeNapoli, F. Cappuzzello, S. E. A. Orrigo, C. Agodi, M. Bondi et al., Phys. Rev. Lett. **118**, 012701 (2017).

[48] G. F. Bertsch, K. Hencken, and H. Esbensen, Phys. Rev. C **57**, 1366 (1998).

[49] J. K. Smith, Unbound states in the lightest island of inversion: neutron decay measurements of ^{11}Li, ^{10}Li, and ^{12}Be, Ph.D. thesis, Michigan State University, 2014 (unpublished), https://publications.nscl.msu.edu/thesis/Smith_2014_362.pdf

[50] F. Marti, P. Miller, D. Poe, M. Steiner, J. Stetson, and X. Y. Wu, in *Cycloctrons and Their Applications 2001: Sixteenth International Conference*, 13–17 May 2001, East Lansing, Michigan, edited by F. Marti, AIP Conf. Proc. No. 600 (AIP, New York, 2001), p. 64.

[51] D. J. Morrissey, B. M. Sherrill, M. Steiner, A. Stolz, and I. Wiedenhoever, Nucl. Instrum. Methods Phys. Res., Sect. B **204**, 90 (2003).

[52] M. D. Bird, S. J. Kenney, J. Toth, H. W. Weijers, J. C. DeKamp, M. Thoennessen, and A. F. Zeller, IEEE Trans. Appl. Supercond. **15**, 1252 (2005).

[53] B. Luther *et al.*, Nucl. Instrum. Methods Phys. Res., Sect. A **505**, 33 (2003).

[54] J. Yurkon, D. Bazin, W. Benenson, D. J. Morrissey, B. M. Sherrill, D. Swan, and R. Swanson, Nucl. Instrum. Methods Phys. Res., Sect. A **422**, 291 (1999).

[55] K. Makino and M. Berz, Nucl. Instrum. Methods Phys. Res., Sect. A **427**, 338 (1999).

[56] N. Frank, A. Schiller, D. Bazin, W. A. Peters, and M. Thoennessen, Nucl. Instrum. Methods Phys. Res., Sect. A **580**, 1478 (2007).

[57] D. Bazin, O. Tarasov, M. Lewitowicz, and O. Sorlin, Nucl. Instrum. Methods Phys. Res., Sect. A **482**, 307 (2002).

[58] Z. Kohley *et al.*, Nucl. Instrum. Methods Phys. Res., Sect. A **682**, 59 (2012).

[59] Y. Aksyutina *et al.*, Phys. Lett. B **666**, 430 (2008).

[60] A. M. Lane and R. G. Thomas, Rev. Mod. Phys. **30**, 257 (1958).

[61] F. Deák, A. Kiss, Z. Seres, G. Caskey, A. Galonsky, and B. Remington, Nucl. Instrum. Methods Phys. Res., Sect. A **258**, 67 (1987).

[62] A. Schiller, N. Frank, T. Baumann, D. Bazin, B. A. Brown, J. Brown *et al.*, Phys. Rev. Lett. **99**, 112501 (2007).

[63] C. R. Hoffman, T. Baumann, D. Bazin, J. Brown, G. Christian, P. A. DeYoung, J. E. Finck, N. Frank, J. Hinnefeld, R. Howes, P. Mears, E. Mosby, S. Mosby, J. Reith, B. Rizzo, W. F. Rogers, G. Peaslee, W. A. Peters, A. Schiller, M. J. Scott, S. L. Tabor, M. Thoennessen, P. J. Voss, and T. Williams, Phys. Rev. Lett. **100**, 152502 (2008).

[64] C. R. Hoffman, T. Baumann, J. Brown, P. A. DeYoung, J. E. Finck, N. Frank *et al.*, Phys. Rev. C **83**, 031303 (2011).

[65] A. Spyrou *et al.*, Phys. Lett. B **683**, 129 (2010).

[66] J. K. Smith *et al.*, Phys. Rev. C **90**, 024309 (2014).

[67] C. Sword *et al.*, Phys. Rev. C **100**, 034323 (2019).

[68] G. Christian, N. Frank, S. Ash, T. Baumann, P. A. DeYoung, J. E. Finck *et al.*, Phys. Rev. C **85**, 034327 (2012).

[69] K. Tshoo, Y. Satou, H. Bhang, S. Choi, T. Nakamura, Y. Kondo *et al.*, Phys. Rev. Lett. **109**, 022501 (2012).

[70] M. Thoennessen, *The Discovery of Isotopes: A Complete Compilation* (Springer, Cham, 2016).